MOL #80176

Cd^{2+} block and permeation in Ca$_V$3.1 (α1G) T-type calcium channels.

A candidate mechanism for Cd^{2+} influx

Kyle V. Lopin, Frank Thévenod, Jessica C. Page, and Stephen W. Jones

Department of Physiology and Biophysics, Case Western Reserve University, Cleveland, Ohio (K.V.L., S.W.J.); Universität Witten/Herdecke, ZBAF, Institut für Physiologie & Pathophysiologie, Witten, Germany (F.T.).; University of Buffalo, Buffalo, New York (J.C.P)

1

Running Title: Cd^{2+} block and permeation in $Ca_V3.1$ T-type calcium channels.

Corresponding Author:

Stephen W. Jones

Department of Physiology and Biophysics

Case Western Reserve University

Cleveland, OH 44106, USA

Phone: (216) 368-5527

Fax: (216) 368-5586

e-mail: swj@case.edu

29 pages

0 tables

10 figures

39 references

163 words in Abstract

443 words in Introduction

908 words in Discussion

Nonstandard abbreviations:

K_D	Dissociation constant
δ	Fractional electrical distance (from the extracellular side)
σ	Surface charge density
τ	Time constant
$P_{O,r}$	Relative P_O

Abstract

Cd^{2+} is an industrial pollutant that can cause cytotoxicity in multiple organs. We have examined the effects of Cd^{2+}_o on permeation and gating in $Ca_v3.1$ (α1G) channels, stably transfected in HEK 293 cells, using whole-cell recording. Using instantaneous I-V currents (measured following strong depolarization) to isolate effects on permeation, Cd^{2+} rapidly blocked currents with 2 mM Ca^{2+} in a voltage-dependent manner. The block caused by Cd^{2+} is relieved at more hyperpolarized potentials, suggesting that Cd^{2+} can permeate through the selectivity filter of the channel into the cytosol. In the absence of other permeant ions (Ca^{2+} and Na^+ replaced by N-methyl D-glucamine) Cd^{2+} carried sizable inward currents through $Ca_v3.1$ channels (210 ± 20 pA at -60 mV with 2 mM Cd^{2+}). $Ca_v3.1$ channels have a significant 'window current' at this voltage ($P_{open} \sim 1\%$) making them a candidate pathway for Cd^{2+} entry into cells during Cd^{2+} exposure. Incubation with radiolabeled $^{109}Cd^{2+}_o$ confirmed that $Ca_v3.1$ channels can lead to the uptake of Cd^{2+}_o into cells.

Introduction

Increasing industrial use of Cd^{2+} has led to widespread contamination of the environment that threatens human health (ATSDR, 2008). The main challenge in the 21st century in a global setting seems to be not acute toxicity but chronic low Cd^{2+} exposure, mainly from dietary sources (Jarup and Akesson, 2009). Ubiquity of Cd^{2+} makes it a serious environmental health problem that needs to be thoroughly assessed because it already affects, or will affect, large proportions of the world's population.

A variety of pathways have been suggested to allow Cd^{2+} entry in excitable and non-excitable cells (Thévenod, 2010). Candidates are DMT1 with a K_m for Cd^{2+} of ~1 µM (Gunshin et al., 1997; Okubo et al., 2003), ZIP8 with a K_m for Cd^{2+} of ~ 0.5 µM (Liu et al., 2008) and ZIP14A/B with a K_m for Cd^{2+} of 0.1-1 µM (Girijashanker et al., 2008). In this context, it is crucial to be aware that blood Cd^{2+} concentrations in the general population are in the range of 1-10 nM (Elinder et al., 1983) and may exceed 100-300 nM in occupationally exposed workers (Hassler et al., 1983). The free Cd^{2+} concentrations in the extracellular fluid that cause tissue damage are unknown but are likely to be in the submicromolar range: Even acute poisoning with oral intake of a high dose of Cd^{2+} result in a Cd^{2+} concentration in the blood of merely ~200 nM (Hung and Chung, 2004). It is not clear whether most studies describing transport of Cd^{2+} have only *in vitro* or mechanistic relevance, or could significantly contribute to *in vivo* toxicity of Cd^{2+}.

T-type calcium channels are blocked by Cd^{2+} (Diaz et al., 2005; Lacinova et al., 2000) but their role in Cd^{2+} transport has not been investigated so far. $Ca_v3.1$ channels may be suitable for Cd^{2+} transport since they have a well-defined window current at negative membrane potentials where the driving force for divalent cation entry is high (Serrano et al., 1999), and $Ca_V3.1$ channels are ~2-fold less selective for Ca^{2+} than L-type calcium channels (Perez-Reyes, 2003) suggesting that Cd^{2+} has an increased chance of permeating the channel in the presence of competing Ca^{2+}. $Ca_V3.1$ calcium channels are expressed in excitable cells, such as neurons,

heart, smooth and skeletal muscle and endocrine cells (Perez-Reyes, 2003). Surprisingly, $Ca_v3.1$

is also expressed in the distal nephron of the kidney (Andreasen et al., 2000), where it may be

involved in Ca^{2+} reabsorption (Leclerc et al., 2004). In this paper we examine Cd^{2+} effects on

gating and permeation of $Ca_v3.1$ channels, and use a model of permeation to estimate the amount

of Cd^{2+} that can permeate through the channels at levels seen during chronic Cd^{2+} exposure.

Materials and Methods

Electrophysiology. Whole-cell patch clamp recordings were made from HEK 293 cells stably transfected with $Ca_V3.1$ calcium channels as described previously (Khan et al., 2008). Electrodes were made from borosilicate glass (World Precision Instruments, Sarasota, FL) and had open-tip resistances of 1.1 to 2.0 MΩ and access resistances upon going whole-cell of 2.0 to 5.0 MΩ. Currents were recorded at room temperature (~21-24 ^{o}C), compensated at 90%, filtered at 10 kHz, and sampled at 50 kHz. Leak and capacitative currents were subtracted using a –P/4 protocol. A holding potential of -100 mV was used to prevent inactivation of the channel. Only cells that had a resting leak less than 200 pA and rundown less than 25% were used. Currents were acquired using an Axopatch 200A amplifier and pClamp 8.2 software (Molecular Devices, Sunnyvale, CA) and analyzed using Clampfit and Matlab.

Recording solutions. The intracellular solution used for all experiments contained (in mM): 2 $CaCl_2$, 1 $MgCl_2$, 120 NaCl, 10 HEPES, 11 EGTA, and 4 Mg-ATP. The pH was adjusted to 7.2 using NaOH. The free Ca^{2+} was calculated as 70 nM. The standard extracellular solution contained (in mM): 2 $CaCl_2$, 135 NaCl, 10 HEPES, and 10 glucose. The pH was adjusted to 7.2 using NaOH. Where indicated $CdCl_2$ was added to the extracellular solution. For the Ba^{2+} data set $BaCl_2$ replaced $CaCl_2$. For the Cd^{2+} permeation data with $NMDG^+$, Na^+ was replaced by $NMDG^+$ and the pH was adjusted using HCl. All chemicals used in the electrophysiology experiments were purchased from Sigma (St. Louis, MO).

Data Analysis. The current through ion channels is affected by two processes, gating and permeation. To separate these two we used an 'instantaneous' current voltage (IIV) protocol to isolate the gating of $Ca_v3.1$ from permeation (Hodgkin and Huxley, 1952). The IIV protocol uses a short (2 msec) pulse to a voltage that will maximally open the channels (+60 mV). The potential is then reset to a wide range of voltages and the initial current measured, see Figure 1A. As the initial pulse will open the same number of channels for each recording, the current-voltage relation is directly proportional to the permeation of ions through a single channel. For

6

determining the effect of added Cd^{2+} on the IIV relationship ('Cd^{2+} block'), currents were converted to chord conductances (Khan et al., 2008) since Cd^{2+} affected the reversal potential and thus the driving force at a particular voltage.

In a second protocol (IV), steps were given from the holding potential to a variable depolarizing potential and the currents were recorded, see Fig. 1B. The currents recorded with the IV protocol are affected by both gating and permeation. Dividing the IV current by the IIV current for each voltage gives the relative open probability ($P_{O,r}$) (Serrano et al., 1999).

Inward currents when Cd^{2+} was the charge carrier were too small to measure. To measure any change in gating in those conditions, channels were activated by a short (2 msec) pulse to varying voltages, and tail currents were measured after the potential was reset to -100 mV, see inset Fig. 9A. As the driving force of the tail currents are the same for each recording, any difference in the currents are proportional to how many channels are opened during the 2 msec voltage step.

For Cd^{2+} block, cells were recorded in control solution (2 mM Ca^{2+}), after the addition of Cd^{2+}, and after return to control solution (washout), Fig. 1A-B. The control and washout currents were averaged to offset any rundown that may have occurred for data on Cd^{2+} block of Ca^{2+} currents. Averaging controls and washout was not done for Cd^{2+} permeation because the cells became very leaky when switched back to Ca^{2+} after being in high levels of Cd^{2+} without Ca^{2+} for periods greater than 2 minutes. To evaluate rundown, briefer Cd^{2+} applications (~30 sec) were performed and, tail currents at -100 mV were measured following brief test pulses, before, during, and after recovery from Cd^{2+}. We estimate that currents reported here for 10 mM Cd^{2+} were reduced by 14 ± 2 % by rundown, and there was no significant change for 2 mM Cd^{2+} (data not shown).

In each condition, data were scaled based on the sum of the IIV currents from +80 mV to -80 mV, to reduce variability from variations in channel expression from cell to cell (Eq. 3 of Khan et al., 2008). For the IIV protocol, the initial amplitudes were estimated from fits to a single exponential equation

$$= A \cdot e^{-t/\tau} + C$$

where A is the initial amplitude, τ is the time constant of decay and C is a constant offset.

Inward currents for the IV protocol were too small to accurately fit to exponential equations in

all but control and 0.3 mM Cd^{2+} conditions. For the IV data the peak currents were measured by

averaging between 2 cursors placed by eye around the peak.

Permeablility ratios. Reversal potentials were calculated by linear interpretation

between the data points on either side of reversal. Permeability ratios were calculated from the

reversal potentials assuming Goldman-Hodgkin-Katz (GHK) theory. For two ions

$$\frac{P_A}{P_B} = \frac{-z_B^2 \cdot \left([B]_i - [B]_o e^{-v_B}\right) \cdot \left(1 - e^{-v_A}\right)}{z_A^2 \cdot \left([A]_i - [A]_o e^{-v_A}\right) \cdot \left(1 - e^{-v_B}\right)}$$

where $v_i = z_i V_r F/RT$ (Frazier et al., 2000). With 3 permeant ions (Cd^{2+}, Ca^{2+}, Na^+) the following

equation can be derived.

$$\frac{P_A}{P_B} = \left[\frac{-P_C \cdot z_C^2 \cdot \left([C]_i - [C]_o e^{-v_C}\right) \cdot \left(1 - e^{-v_B}\right)}{P_B \cdot z_B^2 \cdot \left([B]_i - [B]_o e^{-v_B}\right) \cdot \left(1 - e^{-v_C}\right)} - 1\right] \left[\frac{z_B^2 \cdot \left([B]_i - [B]_o e^{-v_B}\right) \cdot \left(1 - e^{-v_A}\right)}{z_A^2 \cdot \left([A]_i - [A]_o e^{-v_A}\right) \cdot \left(1 - e^{-v_B}\right)}\right]$$

This equation predicts that adding a permeant extracellular ion should cause a more positive

reversal potential.

Gating. To measure the effect of Cd^{2+} on gating, channel activation was measured by

fitting currents from the IV protocol to a fourth power Boltzmann

$$P_{o,r}(V) = \left(\frac{1}{1 + e^{\left(\frac{-(V - V_{0.5})}{k}\right)}}\right)^4$$

where $V_{0.5}$ is the halfway point of activation for an individual voltage sensor and k is the voltage

sensor sensitivity. Voltage shifts in gating caused by Cd^{2+} were calculated (Zhou and Jones,

1995) by subtracting the $V_{0.5}$ for Cd^{2+} activation from the average $V_{0.5}$ for control (2 mM Ca^{2+})

and washout. The Grahame equation was used to calculate voltage shifts from charge screening according to Gouy-Chapman theory (Grahame, 1947).

$$\sigma^2 G^2 = \sum [C_i] \left\{ e^{\frac{-z\Phi}{kT}} - 1 \right\}$$

where G is a constant equal to 270 $\text{Å}^2 e^{-1} \text{M}^{1/2}$ at room temperature, C_i is the concentration of the ith ionic species in solution, z is the valance, k is Boltzmann's constant, T is temperature and σ is the planar charge density. For charge screening without binding σ was set to 1 e^-/ 98 Å^2, as estimated previously (Khan et al., 2008). Binding of Cd^{2+} to the planar charge followed Gouy-Chapman-Stern theory

$$\sigma = \sigma_t \left[1 + K_{Cd}[Cd]_o e^{\frac{-z_i\Phi}{kT}} \right]^{-1}$$

where σ_t was set to 1 e^-/ 98 Å^2, K_{Cd} is the association constant for Cd^{2+} in M^{-1} and σ is the surface charge not neutralized by binding.

Permeation model. We previously reported a 2-site 3-barrier (2S3B) Eyring model for permeation in $Ca_V3.1$ (Lopin et al., 2010). In short, the IIV data collected in this study were normalized to the original data. The parameters for the electrical distances and the energy parameters for Ca^{2+}, Ba^{2+}, Na^+, and Mg^{2+} were fixed to the parameters fitted previously. Parameters for Cd^{2+} were fitted by a least sum of absolute error to all the data points using the Levenberg-Marquardt algorithm.

[109]Cd^{2+} transport. Cellular [109]Cd^{2+} uptake (specific activity 1.5 MBq/μg Cd^{2+}; QSA Global, Braunschweig, Germany) was performed according to a previously described protocol (Erfurt et al., 2003), with some modifications. Briefly, confluent monolayers of HEK293 cells (control, or stably transfected with $Ca_V3.1$) were washed twice with Hank's balanced salt solution with 5.55 mM glucose (HBSS-glucose) before Cd^{2+} incubation. The concentration of $CdCl_2$ (10 mM stock solution in water) was adjusted in HBSS-glucose and labeled with [109]Cd^{2+}

to give a final activity of 18.5 kBq/ml. At specific time points, monolayers were washed with

HBSS-glucose containing 2 mM EGTA (pH 7.0, adjusted with Tris) and solubilized in 1 N

NaOH overnight. ^{109}Cd^{2+} content was determined using a Cobra II Auto-Gamma counter

(Packard Instrument Company, Meriden, CT). Experiments were performed in the absence or

presence of 25 µM NNC 55-0396 (Sigma; 2.5 mM stock dissolved in water), a selective inhibitor

of T-type calcium channels (Huang et al., 2004), to obtain Ca$_V$3.1-specific ^{109}Cd^{2+} uptake.

Throughout the paper data are shown as mean ± sem.

Results

Cd^{2+} is commonly used to block Ca^{2+} currents. To characterize this effect most studies have used voltage steps (Lacinova et al., 2000) and measured the current voltage (IV) relationships, but this reflects effects of Cd^{2+} on both gating and pore block simultaneously. To separate these two effects we have used an 'instantaneous' current voltage (IIV) protocol where a short prepulse is given to maximally open all the channels and the voltage is 'instantaneously' reset and the current measured, as show in Fig 1A,C. Using the IIV protocol the effect of Cd^{2+} on the permeation pathway can be examined in isolation from effects on gating.

Cd^{2+} blocks and permeates through $Ca_v3.1$ channels. Fig. 1A-B shows current records from the IIV and IV protocols, in control (2 mM Ca^{2+} with 145 mM Na^+), with the addition of 300 µM Cd^{2+}, and following wash out. The large voltage range allows both outward Na^+ currents and inward currents carried mainly by Ca^{2+} to be measured. The peak currents for each protocol are shown in Fig. 1C-D for controls and in the presence of three different concentrations of $[Cd^{2+}]$ (0.3, 1, and 3 mM). To determine the voltage dependence of block by Cd^{2+} the chord conductances in the presence of Cd^{2+} were divided by the control value (Fig. 2A). Here it can be clearly seen that as the cell is hyperpolarized the fraction of channels blocked by Cd^{2+} *decreases.* The rate of Cd^{2+} exit out of the pore to the extracellular side will slow as the cell is hyperpolarized, but if the divalent blocker can permeate, then the rate of Cd^{2+} exiting the pore at hyperpolarizing potentials will increase, relieving pore block. As was already noted for Cd^{2+} on $Ca_v3.1$, "Taken together, these results suggest that extreme hyperpolariztion appears to attract Cd^{2+} into the cell" (Diaz et al., 2005). Fig. 2B shows the conductance as a function of Cd^{2+} concentration and voltage. The block saturates at ~85%, as there is an appreciable amount of current that is observed in 3 mM $[Cd^{2+}]_o$. The current remaining could be due to incomplete block of Ca^{2+} currents and/or Cd^{2+} permeation.

Given the voltage dependence of block it is likely that Cd^{2+} decreased currents by getting into and obstructing the pore. To confirm this we changed the charge carrier from Ca^{2+} to Ba^{2+},

11

(Fig. 3). It has been shown previously (Serrano et al., 2000) that due to ion-ion interactions in the pore blockers are more potent when Ba^{2+} is the charge carrier, compared to Ca^{2+}, if the effect of the blocker is on the selectivity filter of the pore. This can clearly be seen in Fig. 3, where Ba^{2+} currents are blocked appreciably more by 300 μM Cd^{2+} than Ca^{2+} currents, either with the IIV protocol (Fig. 3A,C,D) or with the IV protocol (Fig. 3B,E,F).

Since the voltage dependence of block suggested Cd^{2+} permeation, we examined the reversal potentials of the currents after the addition of Cd^{2+}. According to GHK theory, a permeant ion added to the extracellular side should cause a more positive reversal potential. As shown in Fig. 4A, adding $[Cd^{2+}]_e$ actually caused a less positive V_r.

Currents carried by Cd^{2+}. The voltage dependence of block by Cd^{2+} suggests that Cd^{2+} can permeate through the pore. To test this more directly, we recorded currents after replacing 2 mM Ca^{2+} with 2 mM Cd^{2+} (Fig. 5A) and saw sizeable inward currents, shown on an expanded scale in Fig. 5B. To confirm that the currents observed were being carried by Cd^{2+} and not Na^+ we increased the Cd^{2+} concentration to 10 mM. This did not lead to an increase in the current, which might be expected if the currents were being carried by Cd^{2+}. In fact, at very hyperpolarized potentials (-120 mV to -150 mV), the current was less in 10 mM Cd^{2+}. One possibility is that some of the inward current is carried by Na^+, and the higher concentration of Cd^{2+} simply blocks the Na^+ current more effectively.

To eliminate any Na^+ currents that may be mixing in with the Cd^{2+} currents we replaced the extracellular Na^+ with $NMDG^+$, an impermeant cation. Fig. 6 compares currents in 0.2, 2, and 10 mM Cd^{2+} to 2 mM Ca^{2+}. Inward currents increase monotonically with $[Cd^{2+}]$, approaching saturation at 10 mM (Fig. 6B-C). Currents carried by Cd^{2+} were rather large, >200 pA at -60 mV in both 2 and 10 mM $[Cd^{2+}]_o$ (Fig. 6B). This level of current carried through a calcium channel by a 'blocker' is surprising. With the IV protocol (Fig. 6D) inward currents were very small (~30 pA). Using the reversal potentials for Cd^{2+} permeation with NMDG (Figs. 4B, 6B) a permeability ratio of Cd^{2+} to Na^+ ($P_{Cd/Na}$) was calculated as 57.1 using GHK theory

(Fig. 4C). This compares to the $P_{Ca/Na}$ ratio of 87 (Khan et al., 2008). Together this would give a $P_{Cd/Ca}$ of 0.66 where Cd^{2+} is only slightly less permeable than Ca^{2+}, defined using GHK theory.

Cd^{2+} uptake through $Ca_v3.1$. $Ca_v3.1$ channels are known to have a substantial 'window' current, where partial activation combined with incomplete inactivation allows a steady inward Ca^{2+} current near the resting potential (Chemin et al., 2000; Serrano et al., 1999; Williams et al., 1997). The window current is classically measured as the overlap of the activation curve and the inactivation curve. This assumes that inactivation reaches 100% at depolarized potentials. However, inactivation is incomplete for $Ca_V3.1$ channels at all potentials and 1-3% of channels remain open and conduct current (Serrano et al., 1999). The 'window current' predicted by the model is shown in Fig.8F (shown as P_O, dashed line). This window current could be an important source of Cd^{2+} entry into cells. To study if Cd^{2+} can permeate via the window current of $Ca_v3.1$ channels incubation studies were conducted with radiolabeled $^{109}Cd^{2+}$. Experiments were conducted for 30 minutes at varying concentrations of Cd^{2+} in the presence of physiological levels of Ca^{2+}. Cd^{2+} uptake by $Ca_V3.1$ was measured as the difference between cells incubated with Cd^{2+} and cells incubated with Cd^{2+} and the Ca_V3 blocker NNC 55-0396 (Huang et al., 2004). Fig. 7 shows that $Ca_v3.1$ can transport Cd^{2+} into cells at the resting membrane potential in a dose-dependent manner.

Permeation model. To estimate how $Ca_V3.1$ transports trace amounts of Cd^{2+} in physiological conditions, a 2-binding site 3-barrier (2S3B) model was used (Fig. 8). Parameters were estimated by fitting the data on Cd^{2+} block and permeation (Figs. 1, 3, 6) The electrical distances and parameters for Ca^{2+}, Ba^{2+}, Na^+ and Mg^{2+} were fixed to the values used by Lopin et al. (2010). The model was able to effectively describe Cd^{2+} block of Ca^{2+} currents (Fig. 8A), Ba^{2+} currents (Fig 8D) and the permeation of Cd^{2+} (Fig. 8B). However, there is a deviation between the model and data at the most hyperpolarized potentials (-120 to -150 mV) for Cd^{2+} permeation. When Na^+ is replaced by NMDG the current levels off for potentials < -120 mV even when Ca^{2+} is the carrier (Khan et al., 2008, Fig. S20; and compare control currents in Fig

13

6C to Fig. 1C). It is unclear if this is caused by voltage dependent block of $NMDG^+$ or if there are Na^+ currents in addition to Ca^{2+} currents at strong negative voltages (Khan et al., 2008).

The model was used to estimate the transport rate of Cd^{2+} through $Ca_V3.1$ channels as a function of $[Cd^{2+}]_o$ (Fig. 8E). The model predicts that with 3-10 nM Cd^{2+} $Ca_V3.1$ channels can transport on the order of 1 Cd^{2+} ion per second through an open channel. To evaluate the steady-state Cd^{2+} entry rate, the expected steady-state P_O is shown as a function of voltage in Fig. 8F (dashed line, calculated from the model in Serrano et.al., 1999). Notice that the window P_O is constant at depolarized potentials due to incomplete inactivation. Fig. 8F also shows the transport rate through an open channel multiplied by the steady-state P_O; this is the calculated Cd^{2+} transport rate via the window current. The model can also be directly compared to the incubation data by multiplying the transport rate by estimates for the number of cells per well (200,000), number of channels per cell (8,000) (Lopin et al., 2010), and the open probability at rest taking into account slow inactivation* (0.975%), calculated assuming 98.5% fast inactivation (Serrano et al., 1999) and 35% slow inactivation (Hering et al., 2004) at steady-state. All values were taken at -35 mV (Chemin et al., 2000). As shown in Fig. 7, the uptake calculated from the model is very similar to the experimentally observed rate (see Discussion).

Shifts in gating by Cd^{2+}. To determine whether Cd^{2+} affects gating, activation curves were calculated from the Cd^{2+} block data (Fig. 1) using the relative open probability ($P_{O,r}$), calculated by dividing the IV current by the IIV current at each voltage (Serrano et al., 1999) (Fig. 9B). This measurement could not be used for the Cd^{2+} permeation data, as the IV currents were too small to measure accurately (Fig. 6D), so currents were measured from tail currents following brief (2 msec) depolarizations (Fig. 9A). Activation was shifted to more positive voltages in 2 mM Cd^{2+} compared to 2 mM Ca^{2+}. As described previously (Khan et al., 2008), Ca^{2+} causes a voltage shift by interacting with the negatively charged head groups on the cell membrane without binding, i.e. by charge screening or a Gouy-Chapman mechanism (Hille et al., 1975). The additional shift caused by Cd^{2+} compared to an equimolar concentration of Ca^{2+} therefore requires some additional mechanism of action, most likely binding of Cd^{2+} to the

14

channel or cell surface. The simplest such model is a Gouy-Chapman-Stern mechanism, which

allows cations to bind to the surface charges in addition to screening. The voltage shifts caused

by Cd^{2+} are shown in Fig. 10. It can be seen that using $K_A = 0.44$ M^{-1} both the permeation and

block data are described fairly well (solid curves). Binding to surface charge should also shift

the time constants for channel closing to the same degree as the $P_{O,r}$ data. The time constants for

the tail currents of Ca^{2+} currents, and Ca^{2+} currents with the addition of Cd^{2+}, are shown in Fig.

9C. Cd^{2+} caused no change in the inactivation rate (e. g., above 0 mV). There was no clear shift

in the voltage-dependence of channel closing (e. g., below -50 mV), but a slight change in slope

at 1 mM or 3 mM Cd^{2+} . This implies that effects of Cd^{2+} on gating cannot be explained fully by

Gouy-Chapman-Stern theory. The effects of Cd^{2+} on gating in $Ca_v3.1$ should be negligible at

Cd^{2+} concentrations found in the body.

Discussion

In this study, we demonstrate that Cd^{2+} can permeate directly through $Ca_V3.1$ calcium channels. The voltage dependence of Cd^{2+} block of Ca^{2+} currents strongly suggested that Cd^{2+} is a permeant ion, and inward currents were carried by Cd^{2+} in the absence of other extracellular permeant ions. To calculate the rate that Cd^{2+} can permeate $Ca_v3.1$ calcium channels at concentrations seen during Cd^{2+} exposure (3-10 nM) we used a model of permeation, and estimated that ~ 1 Cd^{2+} ion per second can pass through an open channel.

Cd^{2+} permeation and block. Cd^{2+} is classically considered a calcium channel blocker, but previous studies have demonstrated relief of block by hyperpolarization, strong evidence that Cd^{2+} can enter cells via voltage-dependent calcium channels (Brown et al., 1983). This is not surprising in principle, as many divalent cations (including Ca^{2+} itself) can either act as pore blockers or permeant cations, depending on conditions (Almers and McCleskey, 1984; Hess and Tsien, 1984). However, the size of currents carried by Cd^{2+} was surprising, 5-17% of the current carried by Ca^{2+} (comparing both ions at 2 mM; Fig. 6). From reversal potentials with Cd^{2+} (in the absence of Ca^{2+}), the permability ratio is $P_{Cd/Ca} = 0.66$. Note that the permeability ratio primarily reflects the strength of binding, but the actual observed current is also affected by the rate of ion movement through the pore.

Block of $Ca_V3.1$ by Cd^{2+} decreased with hyperpolarization, the reverse of the voltage dependence observed for many other divalents, including Mg^{2+}, Co^{2+}, and Ni^{2+} (Diaz et al., 2005; Obejero-Paz et al., 2008; Serrano et al., 2000). This reflects the relatively strong permeation observed for Cd^{2+}. The relief of Cd^{2+} block by hyperpolarization has also been seen for Ca^{2+} channels in chicken sensory neurons (Swandulla and Armstrong, 1989), suggesting that it could be a common feature of Ca^{2+} channels. Furthermore, based on data with a range of Cd^{2+} concentrations, Cd^{2+} block saturated at 80-85% (Fig. 2), and thus does not completely block currents through $Ca_V3.1$. The remaining currrent is carried in part by Cd^{2+} and in part by Ca^{2+}:

our permeation model predicts that 50-60% of the inward current is carried by Cd^{2+}, with 2 mM Ca^{2+}_o and 3 mM Cd^{2+}_o.

It does not appear that the incomplete block of calcium channels by Cd^{2+} has been noted previously. One factor is that most previous studies have measured inhibition using the IV protocol, instead of the IIV used here. Since Cd^{2+} shifts gating to more positive voltages, inhibition measured by the IV protocol will include both inhibition by pore block and inhibition by lowering channel open probability, which will exaggerate the potency of Cd^{2+} as a pore blocker, and can also exaggerate the maximal extent of pore block (see Fig. 1D). From the experiments examining Cd^{2+} block of Ca^{2+} currents, the reversal potential was shifted to more negative potentials with Cd^{2+}, opposite to expectations from GHK theory. Deviations from GHK behavior are expected for multi-ion pores such as calcium channels, where ion-ion interactions are important.

Permeation model. For the nanomolar concentrations observed in chronic Cd^{2+} exposure *in vivo*, the rate of Cd^{2+} permeation through $Ca_v3.1$ channels cannot be directly measured using electrophysiology. We estimated the transport rate using an Erying rate theory model (Eyring, 1935) of permeation in calcium channels. The model we propose in this paper is a refinement of the original 2-site 3-barrier models of calcium channels (Almers and McCleskey, 1984; Hess and Tsien, 1984) fit to a large data set over various voltages and concentrations of Ca^{2+}, Ba^{2+}, Mg^{2+}, and Na^+ (Lopin et al., 2010). Parameters for Cd^{2+} were estimated by including our data on Cd^{2+} block and permeation. The model can then translate electrophysiological data into transport rates of trace metals through an ion channel under pathophysiological conditions. The model was able to reproduce the $^{109}Cd^{2+}$ uptake data fairly well using previously reported values of the window current and membrane potential. Uncertainties in the resting potential of HEK293 cells, especially with $Ca_v3.1$ channels active (or partially blocked by Cd^{2+}) limit quantitative comparison, but the fraction of $Ca_v3.1$ channels active at steady-state near the assumed resting potential (-35 mV; Chemin et al., 2000) does not depend strongly on voltage (Serrano et al., 1999).

Calcium channels and Cd^{2+} uptake. It is unlikely that there is a dedicated protein to transport Cd^{2+} as it is not a biologically essential metal. Instead Cd^{2+} is transported into cells using mechanisms for other naturally occurring cations such as Ca^{2+} (i.e. 'ionic mimicry' (Bridges and Zalups, 2005; Clarkson, 1993). Cd^{2+} uptake via Ca$_V$3.1 in our study (Fig. 7) is comparable to a previous study with ZIP14 (Girijashanker et al., 2008), but uncertainty in expression levels of different channels and transporters prevents definitive conclusions regarding the relative importance of pathways for Cd^{2+} influx. Previous studies have also linked L-type calcium channels (Hinkle et al., 1987) and the calcium selective TRPC6 channel (Kovacs et al., 2011) to Cd^{2+} uptake. Development of resistance to Cd^{2+} in cell culture has been linked to downregulation of Ca$_V$3.1, suggesting involvement of this channel in Cd^{2+} toxicity (Leslie et al., 2006). Given the large number of calcium channels expressed throughout the body, the importance of Ca^{2+} signaling, and the large number of ions a channel can transport (~10^5 s^{-1}), if a calcium channel is even slightly permeable to Cd^{2+} this could lead to a significant Cd^{2+} entry. This is especially true for Ca$_V$3.1, which has a substantial 'window current' near the resting potential.

Acknowledgements

Authorship Contributions

Participated in research design: Lopin, Thévenod, Jones

Conducted experiments: Lopin, Thevenod, Page

Contributed new reagents or analytical tools: none

Performed data analysis: Lopin, Thévenod, Page, Jones

Wrote or contributed to the writing of the manuscript: Lopin, Thévenod, Jones

References

Almers W and McCleskey EW (1984) Non-selective conductance in calcium channels of frog muscle: calcium selectivity in a single-file pore. *J Physiol (Lond)* **353**: 585-608.

Andreasen D, Jensen BL, Hansen PB, Kwon TH, Nielsen S and Skott O (2000) The alpha(1G)-subunit of a voltage-dependent Ca(2+) channel is localized in rat distal nephron and collecting duct. *Am J Physiol Renal Physiol* **279**(6): F997-F1005.

ATSDR (2008) *Toxicological Profile for Cadmium.* Department of Health and Humans Services, Public Health Service, Centers for Disease Control, Atlanta, GA, U.S.A.

Bridges CC and Zalups RK (2005) Molecular and ionic mimicry and the transport of toxic metals. *Toxicol Appl Pharmacol* **204**(3): 274-308.

Brown AM, Tsuda Y and Wilson DL (1983) A description of activation and conduction in calcium channels based on tail and turn-on current measurements in the snail. *J Physiol (Lond)* **344**: 549-583.

Chemin J, Monteil A, Briquaire C, Richard S, Perez-Reyes E, Nargeot J and Lory P (2000) Overexpression of T-type calcium channels in HEK-293 cells increases intracellular calcium without affecting cellular proliferation. *FEBS Lett* **478**(1-2): 166-172.

Clarkson TW (1993) Molecular and ionic mimicry of toxic metals. *Annu Rev Pharmacol Toxicol* **33**: 545-571.

Diaz D, Bartolo R, Delgadillo DM, Higueldo F and Gomora JC (2005) Contrasting effects of Cd^{2+} and Co^{2+} on the blocking/unblocking of human Ca_V3 channels. *J Membr Biol* **207**(2): 91-105.

Elinder CG, Friberg L, Lind B and Jawaid M (1983) Lead and cadmium levels in blood samples from the general population of Sweden. *Environ Res* **30**(1): 233-253.

Erfurt C, Roussa E and Thévenod F (2003) Apoptosis by Cd2+ or CdMT in proximal tubule cells: different uptake routes and permissive role of endo/lysosomal CdMT uptake. *Am J Physiol Cell Physiol* **285**(6): C1367-C1376.

Eyring H (1935) The activated complex in chemical reactions. *J Chem Phys* **3**: 107-115.

Frazier CJ, George EG and Jones SW (2000) Apparent change in ion selectivity caused by changes in intracellular K^+ during whole-cell recording. *Biophys J* **78**(4): 1872-1880.

Girijashanker K, He L, Soleimani M, Reed JM, Li H, Liu Z, Wang B, Dalton TP and Nebert DW (2008) Slc39a14 gene encodes ZIP14, a metal/bicarbonate symporter: similarities to the ZIP8 transporter. *Mol Pharmacol* **73**(5): 1413-1423.

Grahame DC (1947) The electrical double layer and the theory of electrocapillarity. *Chemical Reviews* **41**: 441-501.

Gunshin H, Mackenzie B, Berger UV, Gunshin Y, Romero MF, Boron WF, Nussberger S, Gollan JL and Hediger MA (1997) Cloning and characterization of a mammalian proton-coupled metal-ion transporter. *Nature* **388**(6641): 482-488.

Hassler E, Lind B and Piscator M (1983) Cadmium in blood and urine related to present and past exposure. A study of workers in an alkaline battery factory. *Br J Ind Med* **40**(4): 420-425.

Hering J, Feltz A and Lambert RC (2004) Slow inactivation of the $Ca_V3.1$ isotype of T- type calcium channels. *J Physiol (Lond)* **555**: 331-334.

Hess P and Tsien RW (1984) Mechanism of ion permeation through calcium channels. *Nature* **309**(5967): 453-456.

Hille B, Woodhull AM and Shapiro BI (1975) Negative surface charge near sodium channels of nerve: divalent ions, monovalent ions, and pH. *Philos Trans R Soc Lond B Biol Sci* **270**(908): 301-318.

Hinkle PM, Kinsella PA and Osterhoudt KC (1987) Cadmium uptake and toxicity via voltage-sensitive calcium channels. *J Biol Chem* **262**(34): 16333-16337.

Hodgkin AL and Huxley AF (1952) The components of membrane conductance in the giant axon of *Loligo*. *J Physiol (Lond)* **116**: 473-496.

Huang L, Keyser BM, Tagmose TM, Hansen JB, Taylor JT, Zhuang H, Zhang M, Ragsdale DS and Li M (2004) NNC 55-0396 [(1S,2S)-2-(2-(N-[(3-benzimidazol-2-yl)propyl]-N-methylamino)ethyl)-6-fluoro-1,2,3,4-tetrahydro-1-isopropyl-2-naphtyl cyclopropanecarboxylate dihydrochloride]: A new selective inhibitor of T-type calcium channels *J Pharmacol Exp Ther* **309**: 193-199.

Hung YM and Chung HM (2004) Acute self-poisoning by ingestion of cadmium and barium. *Nephrol Dial Transplant* **19**(5): 1308-1309.

Jarup L and Akesson A (2009) Current status of cadmium as an environmental health problem. *Toxicol Appl Pharmacol* **238**(3): 201-208.

Khan N, Gray IP, Obejero-Paz CA and Jones SW (2008) Permeation and gating in Ca$_V$3.1 (α1G) T-type calcium channels. Effects of Ca^{2+}, Ba^{2+}, Mg^{2+}, and Na$^+$. *J Gen Physiol* **132**(2): 223-238.

Kovacs G, Danko T, Bergeron MJ, Balazs B, Suzuki Y, Zsembery A and Hediger MA (2011) Heavy metal cations permeate the TRPV6 epithelial cation channel. *Cell Calcium* **49**(1): 43-55.

Lacinova L, Klugbauer N and Hofmann F (2000) Regulation of the calcium channel α_{1G} subunit by divalent cations and organic blockers. *Neuropharmacology* **39**(7): 1254-1266.

Leclerc M, Brunette MG and Couchourel D (2004) Aldosterone enhances renal calcium reabsorption by two types of channels. *Kidney Int* **66**(1): 242-250.

Leslie EM, Liu J, Klaassen CD and Waalkes MP (2006) Acquired cadmium resistance in metallothionein-I/II(-/-) knockout cells: role of the T-type calcium channel Cacnα$_{1G}$ in cadmium uptake. *Mol Pharmacol* **69**(2): 629-639.

Liu Z, Li H, Soleimani M, Girijashanker K, Reed JM, He L, Dalton TP and Nebert DW (2008) Cd^{2+} versus Zn^{2+} uptake by the ZIP8 HCO_3--dependent symporter: kinetics, electrogenicity and trafficking. *Biochem Biophys Res Commun* **365**(4): 814-820.

Lopin KV, Obejero-Paz CA and Jones SW (2010) Evaluation of a two-site, three-barrier model for permeation in $Ca_V3.1$ (α1G) T-type calcium channels: Ca^{2+}, Ba^{2+}, Mg^{2+}, and Na^+. *J Membr Biol* **235**(2): 131-143.

Obejero-Paz CA, Gray IP and Jones SW (2008) Ni^{2+} block of CaV3.1 (α1G) T-type calcium channels. *J Gen Physiol* **132**(2): 239-250.

Okubo M, Yamada K, Hosoyamada M, Shibasaki T and Endou H (2003) Cadmium transport by human Nramp 2 expressed in Xenopus laevis oocytes. *Toxicol Appl Pharmacol* **187**(3): 162-167.

Perez-Reyes E (2003) Molecular physiology of low-voltage-activated T-type calcium channels. *Physiol Rev* **83**(1): 117-161.

Serrano JR, Dashti SR, Perez-Reyes E and Jones SW (2000) Mg^{2+} block unmasks Ca^{2+}/Ba^{2+} selectivity of α1G T-type calcium channels. *Biophys J* **79**(6): 3052-3062.

Serrano JR, Perez-Reyes E and Jones SW (1999) State-dependent inactivation of the α1G T-type calcium channel. *J Gen Physiol* **114**(2): 185-201.

Swandulla D and Armstrong CM (1989) Calcium channel block by cadmium in chicken sensory neurons. *ProcNatlAcadSciUSA* **86**(5): 1736-1740.

Thévenod F (2010) Catch me if you can! Novel aspects of cadmium transport in mammalian cells. *Biometals* **23**(5): 857-875.

Williams SR, Toth TI, Turner JP, Hughes SW and Crunelli V (1997) The 'window' component of the low threshold Ca^{2+} current produces input signal amplification and bistability in cat and rat thalamocortical neurones. *J Physiol (Lond)* **505**(3): 689-705.

Zhou W and Jones SW (1995) Surface charge and calcium channel saturation in bullfrog sympathetic neurons. *J Gen Physiol* **105**(4): 441-462.

Footnotes

Correspondence to Stephen W. Jones, Department of Physiology and Biophysics, Case Western Reserve University, Cleveland, OH 44106.

Kyle V. Lopin and Frank Thévenod contributed equally to this work.

Figure Legends

Fig. 1. Cd^{2+} block of currents through $Ca_v3.1$ channels. A-B, sample IIV and IV records. The protocols are shown below the middle traces. Control currents in 2 mM Ca^{2+} (left), with the addition of 300 µM Cd^{2+} (middle), and after washout (right) are shown. Currents were Gaussian filtered offline to a final -3 dB cutoff of 5 kHz and shown in 20 mV increments. C, 'instantaneous' currents from IIV protocols shown in A, for control and in the presence of 3 concentrations of Cd^{2+} (n=4 for all concentrations). D, peak currents for the IV protocol shown in B (n=4). Symbols in C apply to D.

Fig. 2. Fraction of the chord conductance remaining in Cd^{2+}. A, ratio of the conductance in the presence of Cd^{2+} compared to control as a function of voltage. Data were from IIV measurements as in Fig. 1C (n=4). Symbols as defined in Fig. 1C. B, conductance ratios as a function of $[Cd^{2+}]$. Curves drawn are fits to a single-site model with variable maximal inhibition: 0.11 mM, 84% inhibition (-20 mV), 0.15 mM, 84% inhibition (-40 mV); 0.23 mM, 80% inhibition (-60 mV); 0.36 mM, 80% inhibition. (-80 mV) Data were not well described with a single-site model with 100% maximal inhibition.

Fig. 3. Cd^{2+} block of Ba^{2+} currents. A-B, IIV and IV current records, using the protocol shown below the middle trace. Control currents in 2 mM Ba^{2+} (left), with the addition of 300 µM Cd^{2+} (middle), and after washout (right) are shown. Currents were Gaussian filtered at 5 kHz and shown in 20 mV increments. C, 'instantaneous' currents from the IIV protocol shown in A. D, the fraction of control conductance remaining in 300 µM Cd^{2+} when 2 mM Ca^{2+} or Ba^{2+} was the charge carrier. E, peak currents from the IV protocol shown in B. F, expanded view of the inward currents with the IV protocol. For experiments with Ba^{2+}, n=4.

27

Fig. 4. Effects of Cd^{2+} on reversal potentials. A, effect of addition of Cd^{2+} (to 2 mM Ca^{2+}) on the reversal potential. B, reversal potentials with extracellular Cd^{2+} (0 Ca^{2+}_o, NMDG replacing Na^+_o) and intracellular Na^+. C, fits of P_{Cd}/P_{Na} to GHK theory. The solid line is the best fit, with $P_{Cd}/P_{Na} = 57.1$, and the dashed lines are GHK fits with P_{Cd}/P_{Na} increased or decreased by 50% (85.7 and 28.6). n=4.

Fig. 5. IIV relationships with extracellular Cd^{2+} and Na^+. A, currents recorded when Ca^{2+} was replaced with Cd^{2+}. B, expanded view of A. Note that the currents were larger in 2 mM Cd^{2+} than in 10 mM Cd^{2+} at the most hyperpolarized potentials. n=4.

Fig. 6. Permeation by Cd^{2+}. A, sample current records from the IIV protocol with the extracellular solution containing 2 mM Cd^{2+} and $NMDG^+$. Currents shown were measured between +80 mV and -100 mV in 20 mV increments and are shown after 2 kHz Gaussian filtering offline. B, 'instantaneous' currents from the IIV protocol (as in A) on an expanded scale to show inward currents carried by Cd^{2+} (n=4 for all concentrations). C, same as B but scaled to compare currents carried by Cd^{2+} to Ca^{2+}. D, peak currents measured using the IV protocol (n=4), symbols as in B and C.

Fig. 7. Uptake of Cd^{2+} by HEK cells. NNC 55-0396 (25 µM) sensitive uptake of $^{109}Cd^{2+}$ in untransfected HEK cells, and HEK cells stably expressing $Ca_V3.1$ calcium channels. Cells were incubated for 30 minutes at the indicated concentration of Cd^{2+}. The dashed line is the calculated transport rate for the 2S3B model using the assumptions described in the text. n= 5-9.

Fig. 8. 2-binding site 3-barrier Eyring rate model for Cd^{2+} block and permeation in $Ca_V3.1$ channels. A, fit of the model to IIV relationships where Cd^{2+}_o was added to solutions containing 2 mM Ca^{2+}_o (and $Na^+_{i,o}$). B, fit to IIVs in the absence of Ca^{2+}_o and Na^+_o. C, fit to IIVs with Cd^{2+}_o, zero Ca^{2+}_o, but normal Na^+_o D, fit to IIVs with 2 mM Ba^{2+}_o, and with added 0.3 mM

Cd^{2+}_o. For A-D, symbols are experimental measurements, and curves are model calculations. E, calculated rate of Cd^{2+} influx through an open $Ca_V3.1$ channel as a function of voltage for different $[Cd^{2+}]_o$. F, calculated rate of Cd2+ influx through the window current of Cav3.1 channel as a function of voltage (same symbols as E), dashed line is the open probability of Cav3.1 calculated from the model in Seranno et.al. 1999. G, energy profiles for the ions included in the model. The energy levels for Cd^{2+} in kT units, from outside to inside, are 8.56, -14.46, 2.17, -11.10, and 14.49. Other parameters are from Table 1 of Lopin et al. (2010).

Fig. 9. Effects of Cd^{2+} on gating. A, activation measured from tail currents after 2 msec prepulses (n=4), normalized to the tail currents following steps to +100 mV B, activation curves calculated by dividing the peak IV current by the IIV current (n=4). C, time constants of the tail currents using the IIV protocol (n=4).

Fig. 10. Voltage shifts induced by Cd^{2+}, fitted to Gouy-Chapman-Stern theory using the Grahame equation. The solid curves are the fit of both Cd^{2+} block and permeation data to the same K_A (0.4435 M^{-1}). The fit is fairly good to both data sets considering different methods were used to measure the $P_{O,r}$ (Fig. 9). The best fits to the data sets separately were 0.85 M^{-1} for block, and 0.26 M^{-1} for permeation (dashed curves).
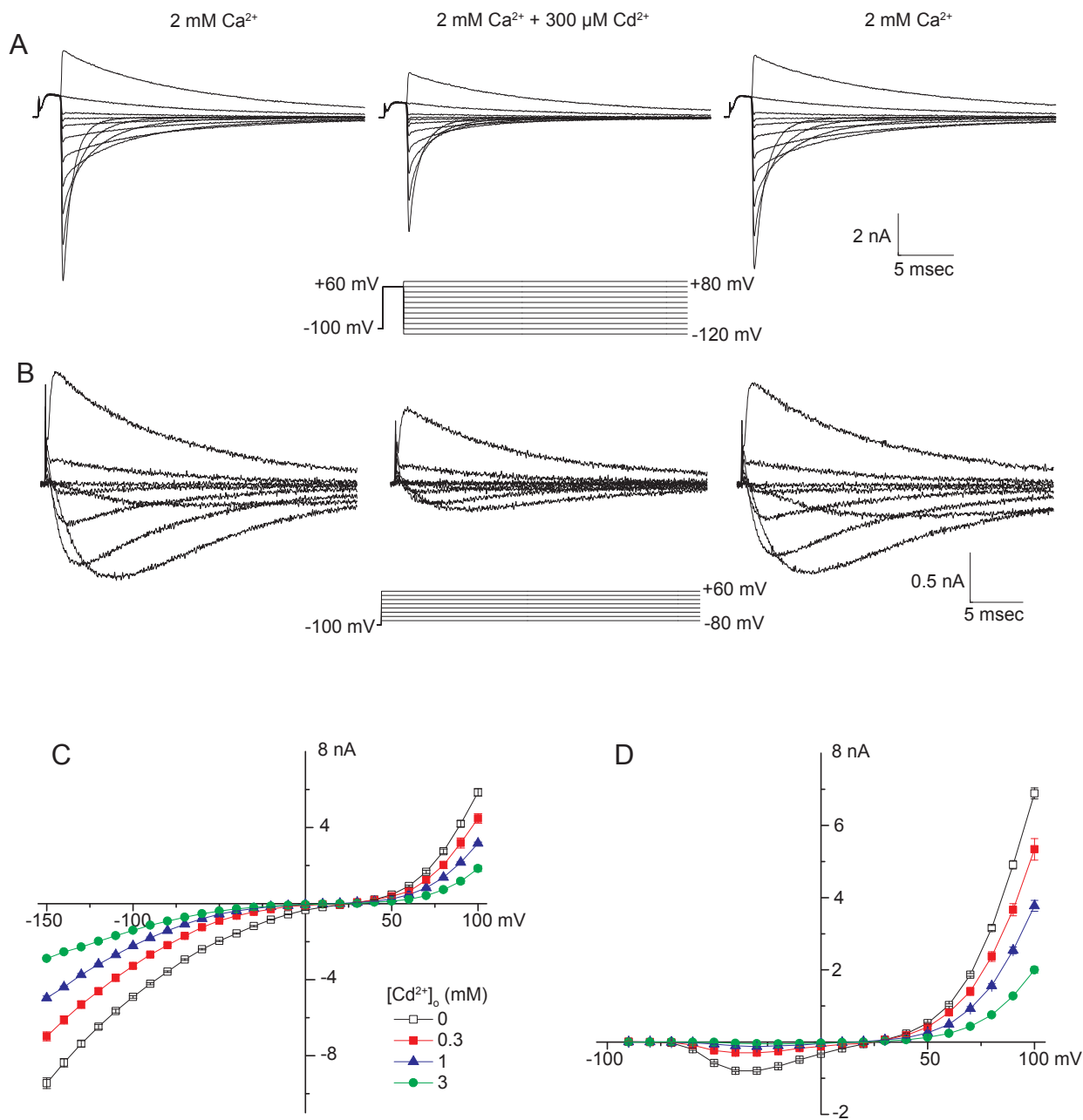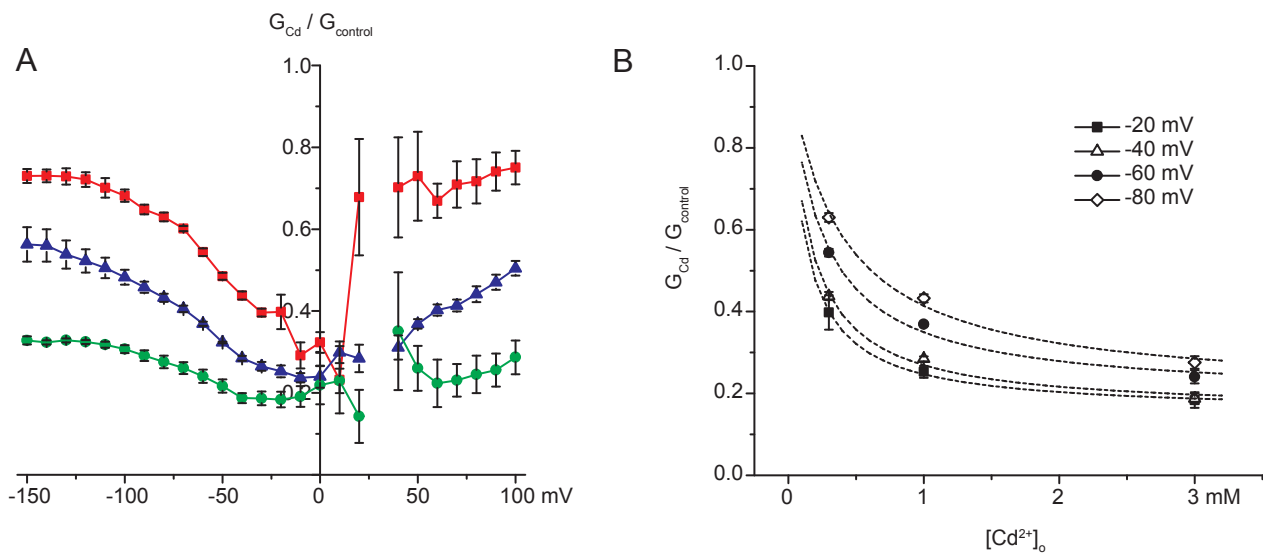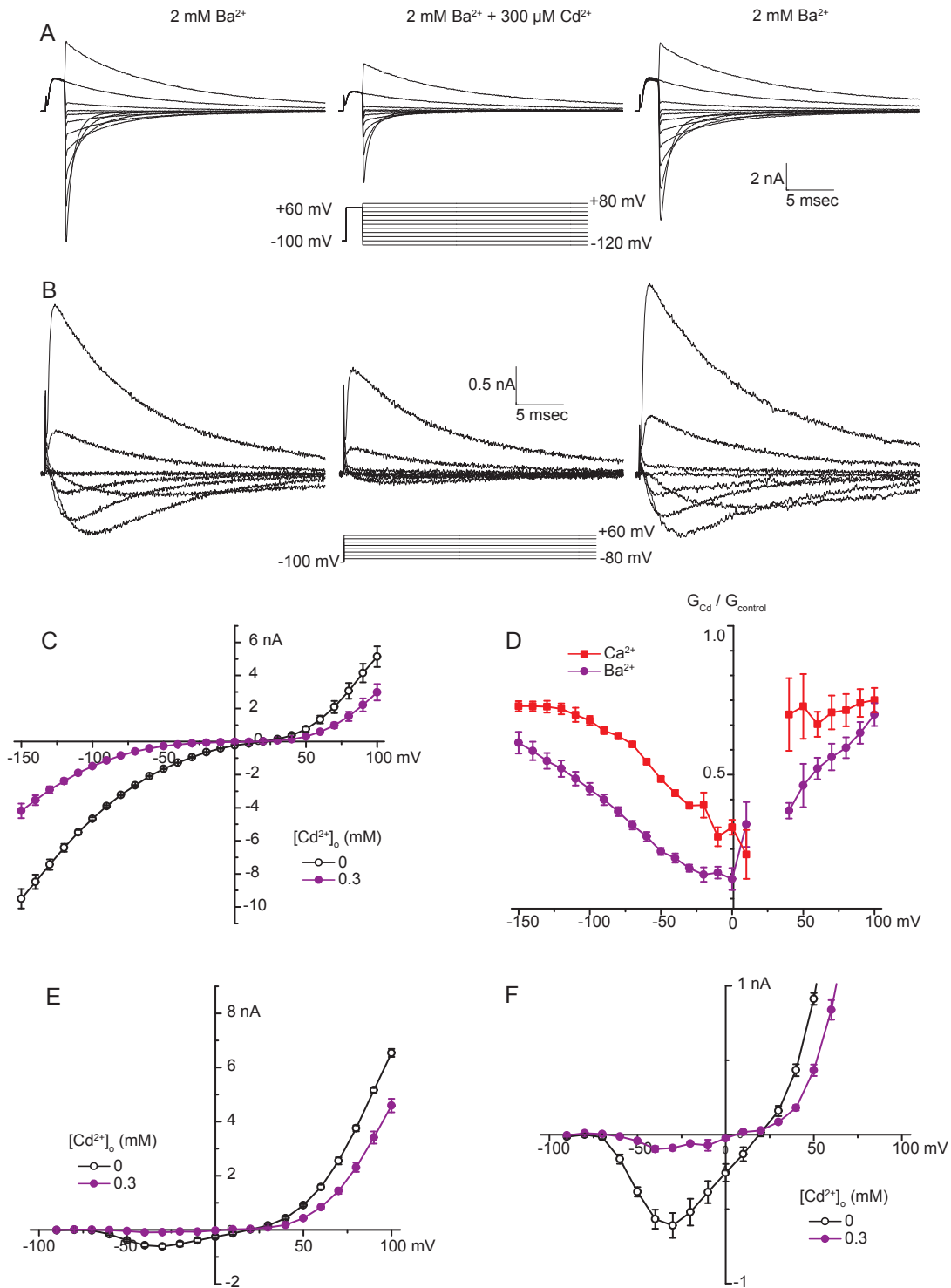
Figure 1

Figure 2

Figure 3

Figure 4

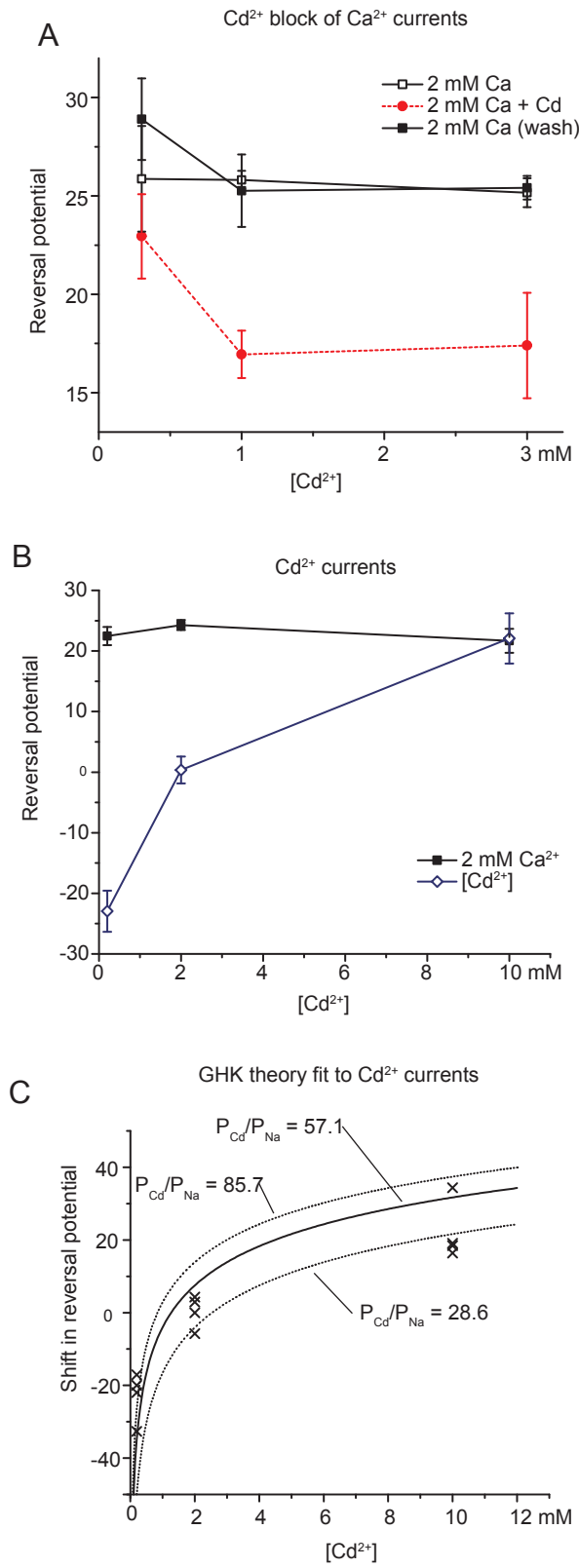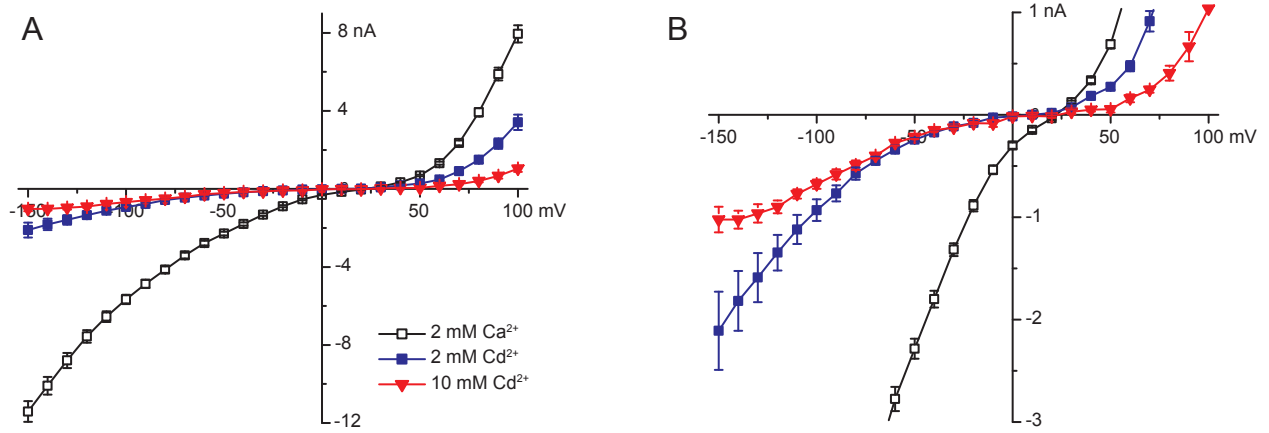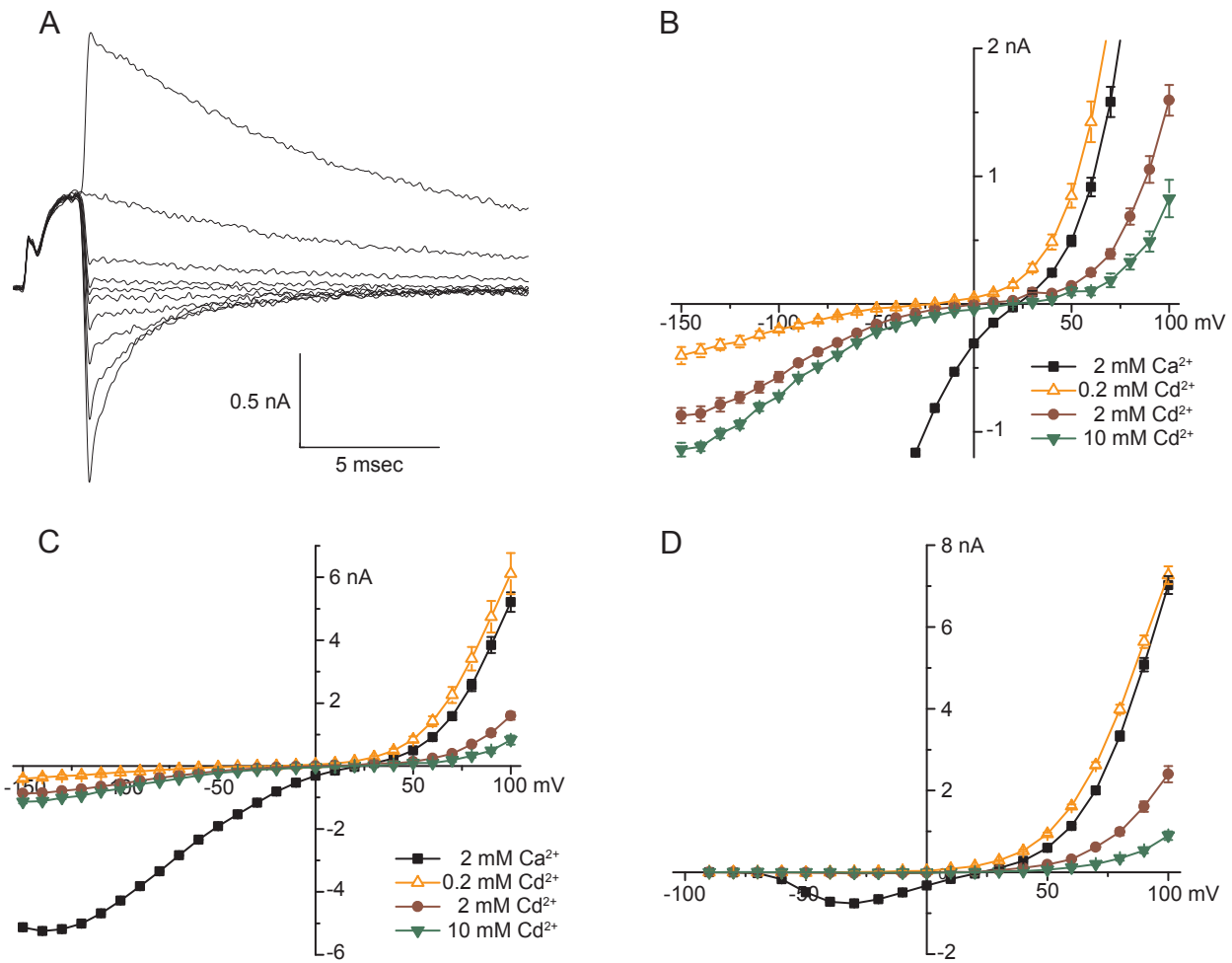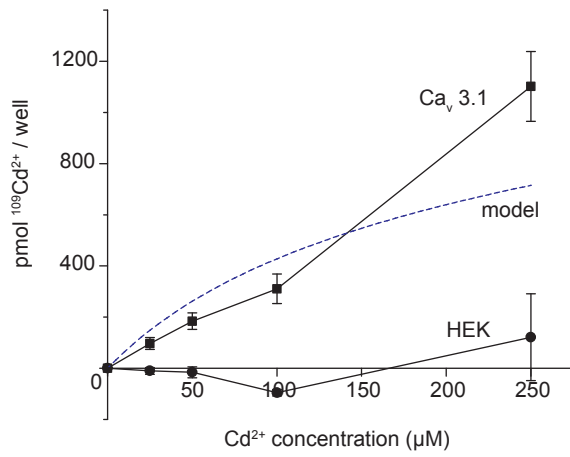A. Cd²⁺ block of Ca²⁺ currents
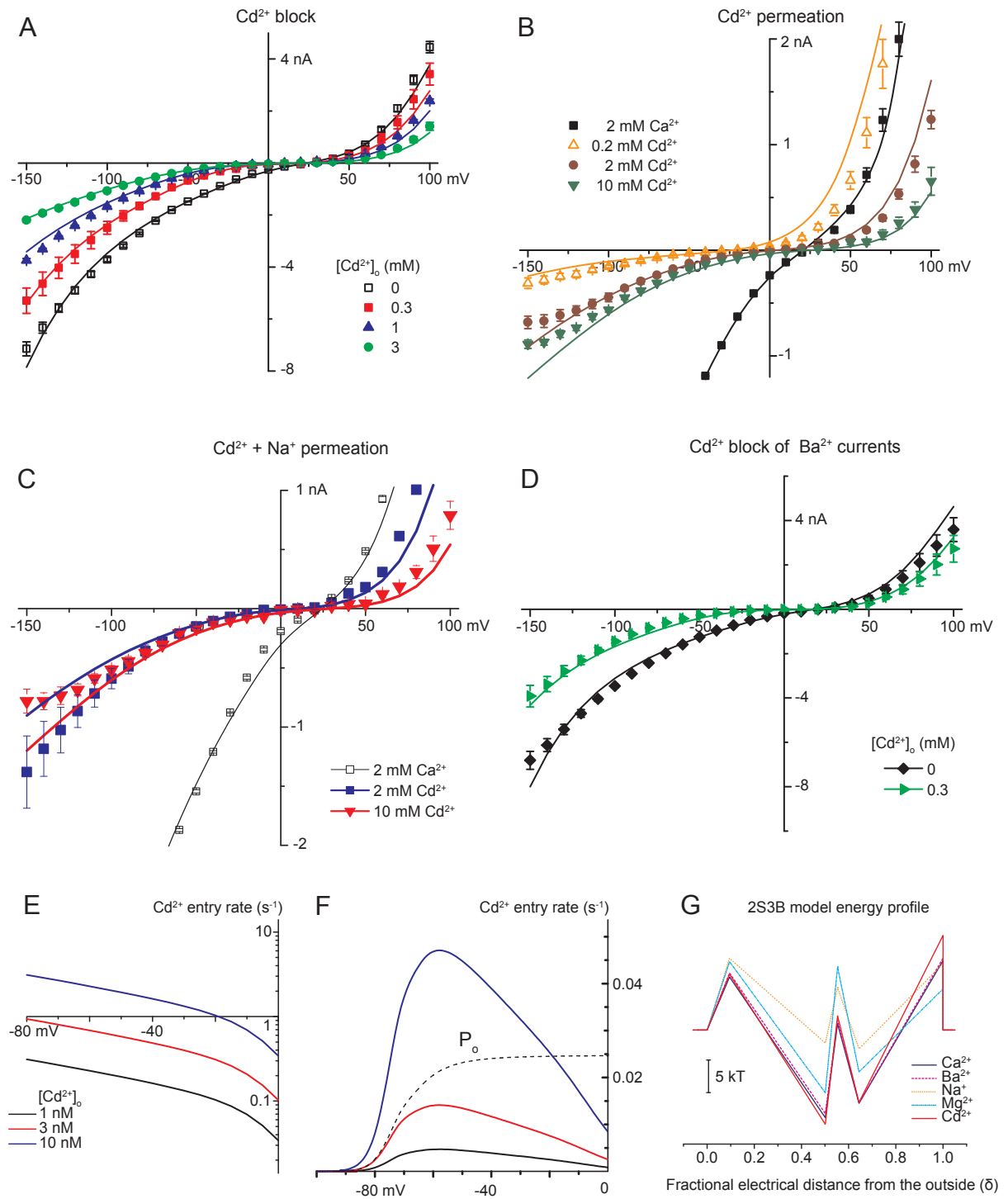
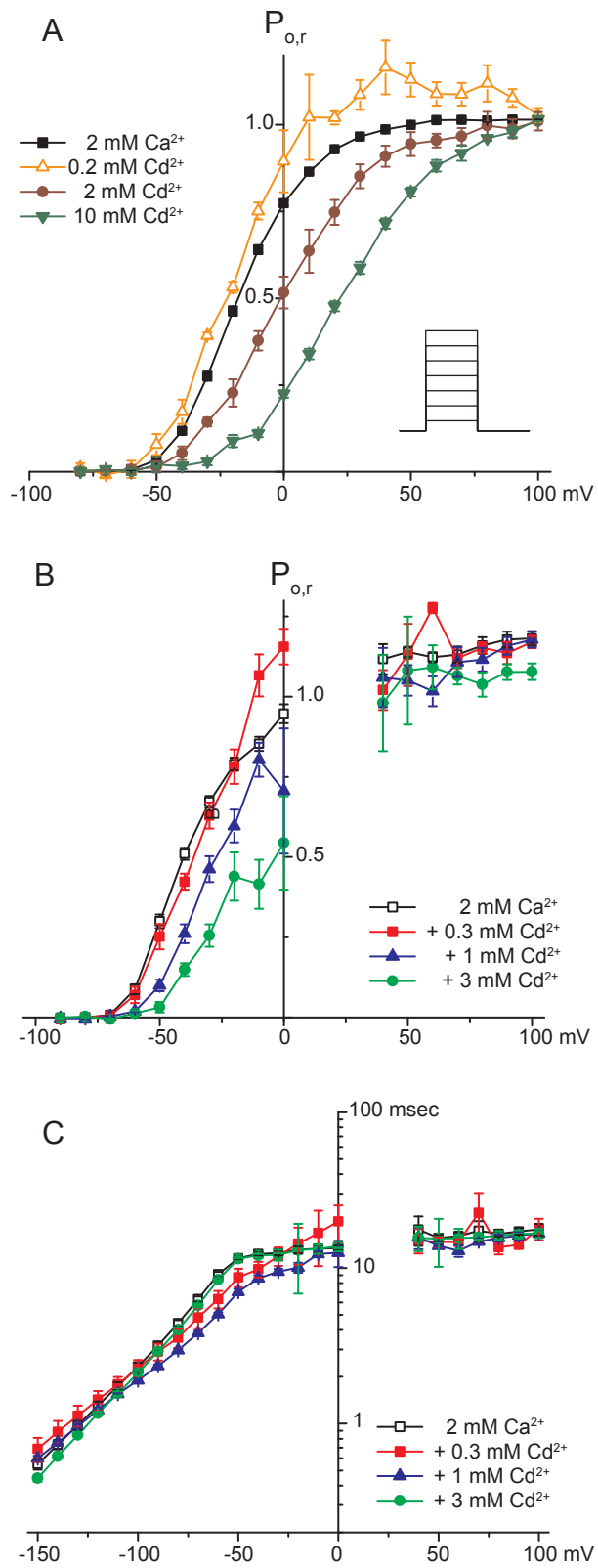B. Cd²⁺ currents

C. GHK theory fit to Cd²⁺ currents

Figure 5

Figure 6

Figure 7

Figure 8

Figure 9

Figure 10